Rock Mechanics
and Rock Engineering 25, 25—47

Rock Mechanics and Rock Engineering

Experimental Study of Fracture Processes in Rock

By

A. K. Maji and **J. L. Wang**

Department of Civil Engineering, University of New Mexico, Albuquerque, U. S. A.

Summary

The Fracture process zone in compact tension specimens of Indiana limestone was investigated to study its effect on the fracture mechanics parameters in such materials. Specimens were tested up to the peak load, and propagation of the crack from a preexisting notch was monitored. Experiments were designed to study the two features of the fracture process zone in rocks: ligament connections and microcracking.

To observe this zone with high sensitivity and accuracy, laser interferometry methods were adopted. Holographic Interferometry was used to observe initial crack propagation. To obtain more quantitative measurements of the displacement field, in realtime, the recently developed technique of electronic speckle pattern interferometry was applied. This technique can provide continuous video recording of the interferometric fringe pattern, depict the evolution of the fracture process, and measure profiles of crack opening displacements.

The macroscopic observations of full-field displacement by the laser techniques were supplemented by post mortem observation of the fractured region under a scanning electron microscope. Regions around the crack were studied after the test for possible presence of microcracks.

An interactive finite element code was used to compute the stress intensity factors of the propagating crack-tip and displacements. Finite element computations were used to evaluate the effect of the process zone on crack propagation.

1. Introduction

Linear Elastic Fracture Mechanics (LEFM) has been applied by several researchers to understand crack propagation in rocks. However, the applicability of LEFM to materials like rocks, concrete and ceramics is open to question. LEFM is applicable to perfectly brittle materials where the material behaves elastically till it fractures. In that case, energy from applied loading is converted to elastic strain energy and surface energy due to the formation of a main crack (Griffith, 1921). However, rocks are not perfectly brittle and exhibit pre-peak nonlinearity and post-peak unloading

called "strain softening" (Labuz et al., 1985; Ouchterlony, 1982). The two physical phenomena that are considered to be responsible for this behavior are: 1. microcracking near the crack tip, and 2. ligament connection or crack bridging across the main crack due to aggregate interlock, unbroken fibre etc. In metals, energy is dissipated by plastic deformation prior to fracture. Therefore the validity of LEFM in metals, concrete or rocks depend upon whether or not the inelastic effects due to plasticity, microcracking or ligament connection are negligible in comparison to the elastic energy and the surface energy. Also, LEFM assumes that the material is homogeneous, whereas rocks can perhaps be considered homogeneous only at a scale much larger than the grain size. Therefore the applicability of LEFM depends on the size of the specimen and the crack (Mindess, 1983).

It is suggested that the crack propagation in rocks, concrete, etc. is associated with the formation of microcracks at the crack tip, and interlocking of particles behind the crack tip (also called ligament connection or crack bridging). These phenomena are different from the plastic yielding near the crack tip in metals. The validity of LEFM in these materials

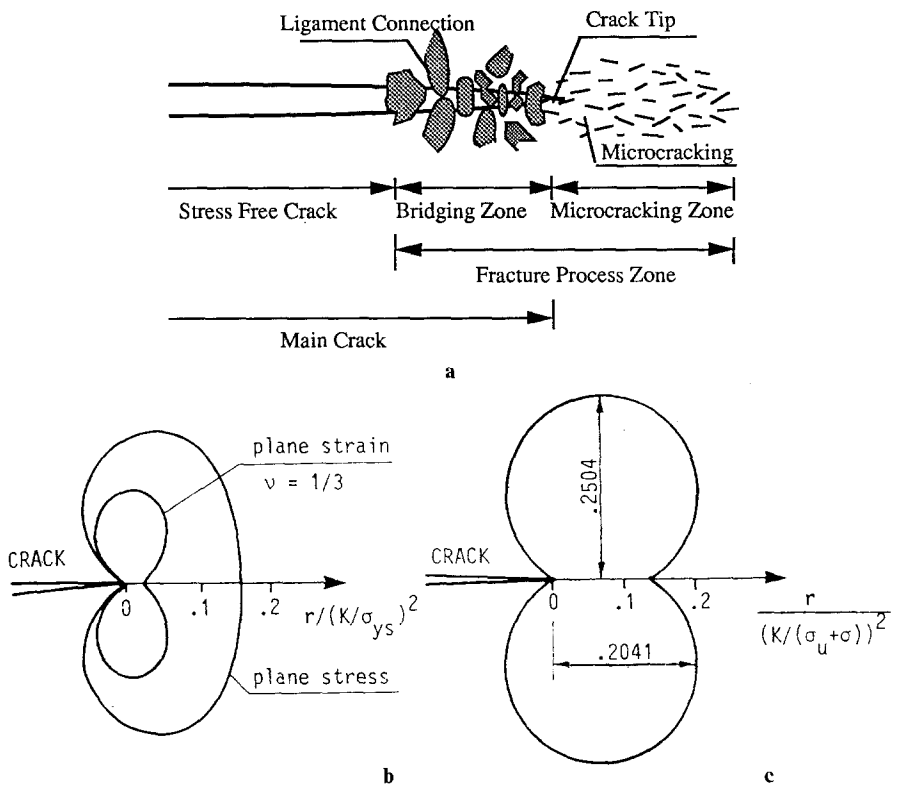

Fig. 1. Theoretical models of process zone. **a** Fracture prozess zone, **b** Plasticity model, **c** Maximum tensile stress criterion

depends on the effects of these features on crack propagation. In concrete, rocks, etc., the region near the crack tip (Fig. 1a) containing the micro-cracked zone and the ligament connections is called the fracture process zone (FPZ). The effect of the fracture process zone (FPZ) on the propagation of a tensile crack has been a subject of considerable interest over the years, and is the subject of this research.

For fracture testing in metals, it is required that this process zone (zone of plastic deformations in metals) should be significantly smaller than any of the dimensions of the specimen (size, crack length etc.). The nonlinear effects of the plastic zone can then be neglected under such situations called "small scale yielding". A similar concept is applied to rocks where the process zone has to be much smaller than the length of the crack for LEFM to be useful. This also relates to the grain size of the rock which is related to the process zone length. While LEFM might be valid for fine grained rocks of a certain size, it might not be valid for rocks with larger grain size, or for specimens of small dimensions. It has, however, been demonstrated by several researchers that the process zone size in concrete, rocks, etc. is large enough for it to be necessary to include its effect in studying the fracture of laboratory size specimens (Hoagland et al., 1973; Bazant, 1985). Therefore, in order to make predictions on crack propagation, it is necessary to study the effects of the FPZ on the fracture mechanics parameters and on crack propagation.

In this study it was necessary to observe the effect of ligament connection and crack length on the specimen deformation and the stress intensity factor at the crack tip. Since there were no closed form equations available, it was necessary to use a finite element code to evaluate the necessary quantities.

The research reported here had four objectives:

1. To observe and quantify the crack propagation and the features of the FPZ using nondestructive testing techniques; laser interferometry and scanning electron microscopy.
2. To study the effect of crack propagation, ligament connection etc. on the fracture mechanics parameters, using a finite element code.
3. To experimentally measure the effects of the FPZ on the crack propagation parameters related to LEFM.
4. To observe the relative importance of ligament connections and micro-cracking.

2. Process Zone Models

Evaluation of the process zone dimensions and physical characteristics of the nonlinear behavior of rocks have been modeled by several researchers. Details of various experimental studies have been summarized by Ouchterlony (1982). Schmidt (1976, 1979) suggested that the crack length "a" should be larger than 2.5 $(K_{Ic}/\sigma_t)^2$, where K_{Ic} is the critical Stress Intensity

Factor (SIF), and σ_t is the tensile strength of the rock. This equation was obtained from ASTM standards for metals, and from a calculation of the plane strain plastic zone at the crack tip for metals (McClintock and Irwin, 1965), which has an extension of (Fig. 1b):

$$r = 0.13\,(K_{Ic}/\sigma_y)^2 \tag{1}$$

where σ_y is the yield stress of the metal.

Typical experimental data on Indiana Limestone were obtained by Schmidt (1976): $K_{Ic} = 750$ psi$\sqrt{\text{in}}$ and $\sigma_t = 750$ psi. These numbers substituted in Eq. (1), results in a size of $r = 0.13''$ (0.33 cm). Using the same data to interpret the ASTM requirement that: $a > 2.5\ (K_{Ic}/\sigma_t)^2$, mentioned above, means that "a" should be larger than 2.5″ (6.35 cm).

Estimation of the size of the process zone varies depending on plane-stress or plane-strain conditions in metals. If the maximum tensile stress criterion is used for rocks instead of the plastic yield criterion used for metals, the size and shape of the microcrack zone becomes different (Fig. 1c). As observed in this figure, the process zone is expected to extend more to each side of the crack than it extends in front of the crack-tip.

Dugdale (1960) used a closing pressure model, where the process zone was modeled as a crack under a uniform closing pressure of magnitude σ_y. It was realized that, in case of rocks, microcracking and crack bridging by ligaments contribute to the process zone. Hence, to model the effect of ligament connection, Barenblatt (1962) introduced a general closing pressure model that is more representative of the strain softening behavior of rocks. Using these models, the dimensions of the process zone, under plane stress conditions were estimated to be

$$r = 0.39\,(K_{Ic}/\sigma_y)^2 \text{ and } 0.88\,(K_{Ic}/\sigma_t)^2 \tag{2}$$

respectively.

Contrary to the above mentioned models, Ballarini et al. (1984) assumed that a stress singularity exists at the effective crack tip. The process zone was found to be about 40% of the stress-free crack length. Jenq and Shah (1985) used an effective crack length model to calculate a modified stress intensity factor (SIF) in concrete. The effective crack length reported by them ranged from about 10% of the original crack length for 3″ notch specimens, to about 100% of the original crack length, for 1″ notch specimens. Labuz et al. (1985) also used the effective crack length model and estimated the process zone size of Charcoal and Rockville Granite. They were able to detect a pre-peak crack propagation of only about 1 mm using quantitative optical microscopy on Double Edge Notched, Charcoal granite specimens. They also observed, that the larger grain size in Rockville granite results in a larger process zone size.

On the other hand, Boone et al. (1986) have demonstrated through numerical computations using a closing pressure model that the process zone has a far greater physical dimension and extends throughout the specimen during progressive strain softening. This would imply that true

small scale yielding or LEFM conditions are never met, which makes a study of the process zone all the more important. Their results, however, are from numerical computations only, and no physical evidence is provided.

3. Experimental Background

Mindess (1991) has provided an overview discussing the pros and cons of the different experimental approaches to study the process zone. Rossmanith (1983) has provided an overview of the various fracture tests conducted on rocks. However, experimental techniques to detect and quantify the physical characteristics of this zone have numerous shortcomings, and few nondestructive evaluation tools have been applied to study the process zone in rocks.

Conventional techniques such as strain gaging (Chhuy et al., 1986) or microscopy (Diamond and Bentur, 1985) can monitor only a very limited area. Nolen-Hoeksema and Gordon (1987) have used a reflecting light microscope to observe crack propagation in dolomite marble specimens. X-ray techniques can survey a large area, but do not have adequate resolution to capture microcracking or any cracks of small openings (Najjar et al., 1988). Photoelasticity and Moire techniques (Du et al., 1989) have the full-field capability, but require special surface preparations and are not strictly noninvasive. Kobayashi and Fourney (1978) used the replicate film technique to study progressive cracking in Westerly granite. The acoustic emission technique has been used to capture microfracture events in Westerly granite under compressive loading in real-time. But, the source locations techniques (Getting et al., 1986) are not accurate enough to detect the crack tip locations. In order to capture the physical phenomena related to fracture and LEFM, it is necessary to develop techniques that can monitor and quantify a progressing crack with high precision without influencing the specimen's behavior.

Two Laser Interferometry Techniques, Holographic Interferometry (HI) and Electronic Speckle Pattern Interferometry (ESPI) were therefore adopted in our experiment due to their full-field, non-invasive nature and high sensitivity. These techniques have a displacement resolution of a fraction of the wavelength of the laser (0.63 micrometers for the Helium-Neon laser used here). Cracks as small as 0.25 micrometers can be observed. The length of the cracks that can be measured does not have any particular limitations.

Holographic Interferometry (HI) has been applied by various researchers to study deformation fields on concrete (Jacquot and Rastogi, 1983). Maji and Shah (1990) have used quantitative HI to observe mixed-mode crack propagation in mortar. They were able to measure crack opening and sliding displacements and study the effect of crack surface tractions in the process zone. Miller et al. (1988) used sandwich holography to quantitatively measure tensile fracture in mortar specimens. A summary

of different laser interferometry techniques and experimental methodology have been described elsewhere by Maji and Shah (1991). Park and Jung (1988) have used HI to study creep deformation of Shale, Sandstone and Coal in a three-point loading apparatus, which was mounted on an optical table. Swanson (1984) used HI to study cracks in Westerly granite and Ralston Besalt. Although numerous experiments have been conducted on concrete using HI, there has been very little implementation of the technique in the rock mechanics area.

3.1 Holographic Interferometry

In Holographic Interferometry, a laser light is divided into two parts, one of which (called the reference beam) is made to shine directly on a photosensitive holographic plate (on the plate holder). The other part of the light (called the object beam) is shone on the specimen from which it is diffusely reflected to the same holographic plate. The path of the different beams and the instrumentation are shown in Fig. 2. The interference between the two beams results in a hologram being created on the plate. In our work the "double exposure" technique was used. This involved making two holograms at two stages of loading of the specimen on the same holographic plate. The resulting hologram then contains fringe patterns corresponding to the difference in the displacement field on the specimen between the two loading stages. These fringes are representative of the displacement component along the "sensitivity vector", which is the bisector of the illumination and the observation direction of any point on

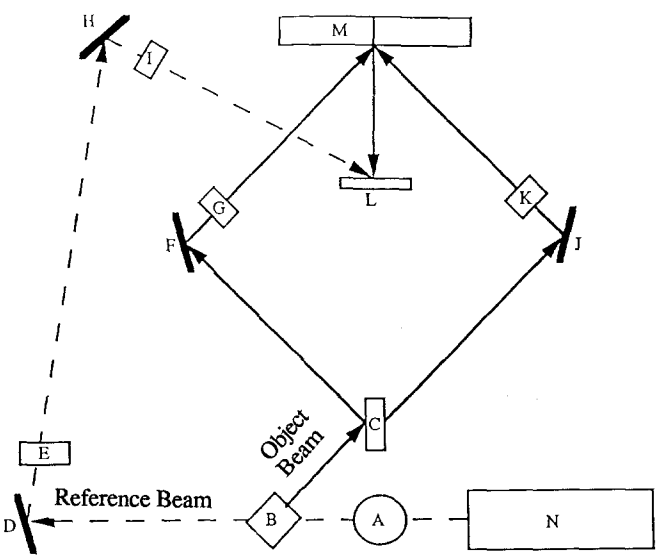

Fig. 2. Schematic diagram of holographic interferometry (HI) setup
Beam steering mirror (*A*), beam-splitter (*B, C, E*), mirrors (*D, F, H, J*), spatial filters (*I, G, K*), plate holder (*L*), specimen (*M*), He-Ne laser (*N*)

the specimen. Cracks are visible as discontinuities or distortions of the fringe pattern. Typically a single object beam is used. In our work two object beams were used for reasons that are described next.

3.2 Symmetric Illumination Holographic Interferometry Set-up

The optical setup used for HI in our experiment used two beams to illuminate the specimen (Fig. 2). Figure 3 is a photograph of the actual test setup. The two beams were symmetric to the out-of-plane direction of the specimen at the notch. The advantage of the set-up is that, contrary to usual out-of-plane sensitivity of HI, illumination with two symmetric beams creates fringe patterns corresponding to in-plane displacements, and reduces out-of-plane sensitivity. Regnault and Bruhwiler (1988), have used this set-up to study the process zone in concrete, during wedge splitting tests.

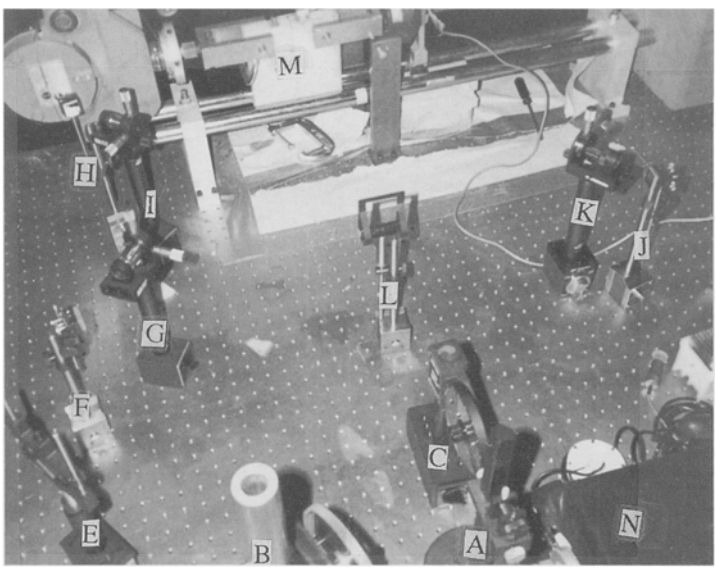

Fig. 3. Loading frame and holographic interferometry (HI) optical setup on vibration isolation table

Beam steering mirror (*A*), beam-splitter (*B, C, E*), mirrors (*D, F, H, J*), spatial filters (*I, G, K*), plate holder (*L*), specimen (*M*), He-Ne laser (*N*)

A 30 mw continuous wave Helium-Neon (He-Ne) laser was used. A shutter arrangement was fixed to the laser so as to eliminate any light in the room while the shutter was off. This was necessary, because replacing holographic plates on the plate holder and other associated tasks took considerable time, which might have caused some unwanted exposure to the plate.

3.3 Electronic Speckle Pattern Interferometry (ESPI)

The HI setup, although useful in observing crack initiation and propagation, was not suitable for measuring crack openings because of spurious rigid body motions of the specimen. The ESPI technique was therefore used for quantitative measurements, because it is less sensitive to out-of-plane motions. This technique, first demonstrated by Butters and Leendertz (1971), combines laser interferometry with image processing to create a more versatile method of nondestructive testing. Jones and Wykes (1983) have provided a detailed description of the pros and cons of the technique. The experimental setup is shown in Fig. 4. The laser beam is split into two parts, each of which is used to illuminate the specimen from symmetrical directions. The natural roughness of the specimen surface under illumination produces tiny spots of light and dark called "speckles". The speckles are therefore caused by the specimen surface under laser illumination and hence, no special specimen preparation is necessary, and the technique is strictly non-invasive. When a TV camera is focused on the specimen, the specimen and the speckles are focused on the image plane of the camera. A CCD camera used for this experiment then digitizes and stores this speckled image. The images are acquired and stored with the help of an image analysis system operated with an IBM-AT computer.

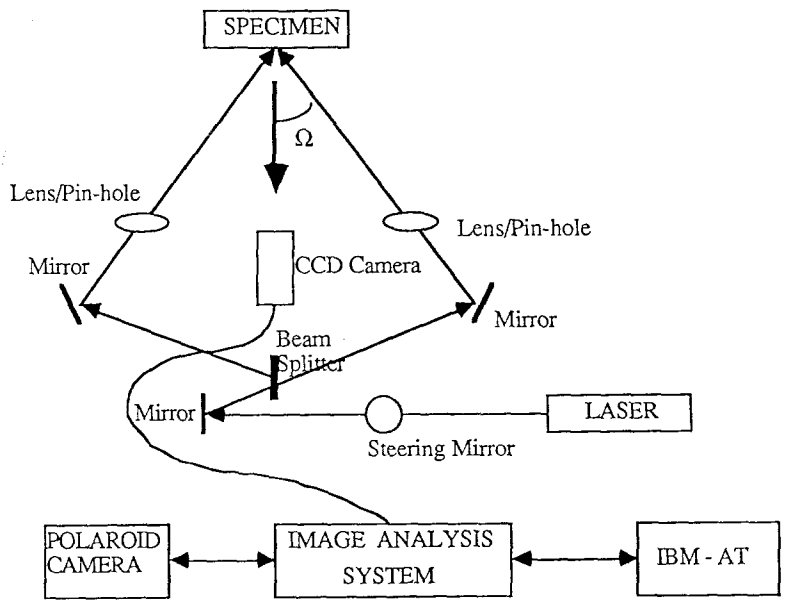

Fig. 4. Schematic of the electronic speckle pattern interferometry setup

Due to the symmetric illumination, out-of-plane object motion causes the same change in path length for the two illumination beams. The ESPI technique is therefore suitable for in-plane measurements and is relatively insensitive to the out-of-plane deformations (Jacquot and Rastogi, 1983).

The image analysis system was first used to obtain a reference image. The camera scans at the rate of 25 frames/second. Hence, the vibration isolation requirements of ESPI are far less stringent than in holography or conventional speckle methods, which involve relatively long exposures of the films. An image analysis software "Imaster" was used in the "Real-Time Acquisition" mode. An image of the specimen was first acquired and stored in computer memory. This image was automatically substracted from all subsequent images being acquired, in real-time by the Imaster software. As a result, the fringe patterns corresponding to the interference between the first image and subsequent images could be observed in real-time. At any point of loading the fringe pattern could be frozen and stored in memory for further processing.

Typically, a reference image is first acquired. The specimens are then loaded and the fringes gradually increase in number as the deformation increases. The fringe patterns are stored in memory at a certain stage of loading and the load is recorded. Another reference image is then made at that load and the process continues. Many fringe patterns (about 30) are recorded for each specimen loaded to failure, and they are processed and analyzed later. Post-processing of the images involves frequency domain filtering, smoothing etc. to improve fringe visibility. Hard copy output of the images was then obtained by a "Polaroid Freeze-Frame Video Recorder".

A 4″ × 3″ (10.16 cm × 7.62 cm) area on the specimen near the notch was studied with the ESPI technique. It was not possible to illuminate the entire specimen with the available laser light without degrading the images.

3.4 Scanning Electron Microscopy

While the laser interferometric studies provide highly sensitive full-field data, they do not provide any information on the microscopic nature of the fracture process. SEM studies were therefore conducted on the already tested specimens to observe the nature of cracking. Specimens tested were cut into 2″ × 2″ (5.1 cm × 5.1 cm) blocks with a diamond saw. The saw cuts were away from the crack and the cutting process was then not likely to influence the process zone. The specimens were carbon coated to prevent charge build-up and were placed in the SEM chamber. The SEM was used to observe various sections in the vicinity of the propagated crack with magnifications ranging from 60 to 1900. The objective of this study was to observe the tortuous nature of the crack, crack bridging by grains, possible existence of microcracking adjacent to the crack etc.

4. Test Set-up

4.1 Testing Fixtures

The experimental set-up used in these tests was similar to that used by Miller et al. (1988). A 4′ × 6′ pneumatic vibration isolation table was used, which was housed in a 9′ × 10′ × 7′ lightproof frame. Nitrogen gas cylinders, pressure regulator and filter were needed to operate the pneu-

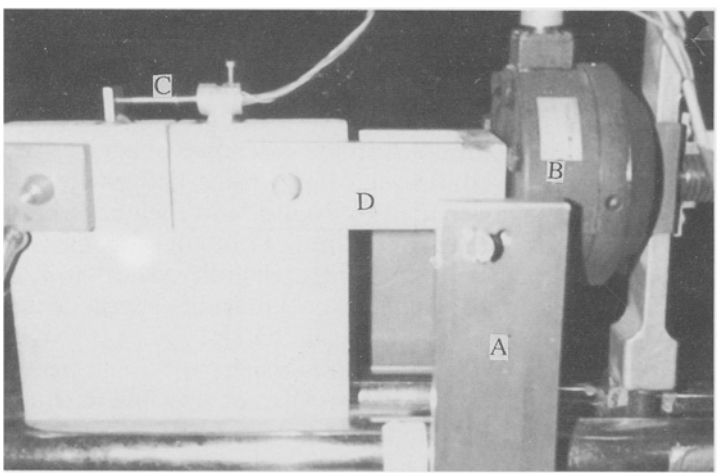

Fig. 5a. Test specimen in loading cell
Clamp (*A*), load cell (*B*), LVDT (*C*), loading grips (*D*)

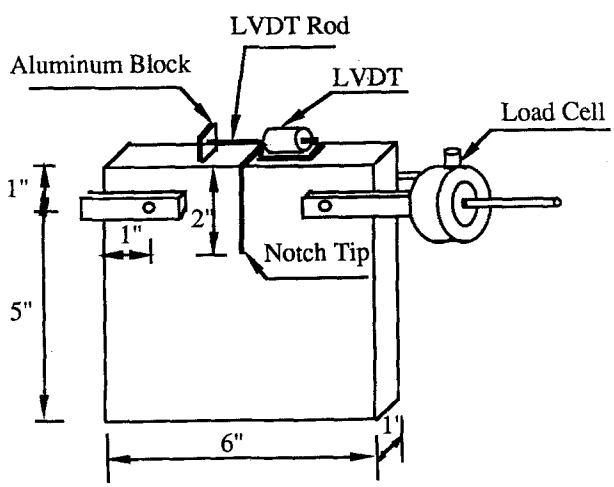

Fig. 5b. Schematic of specimen and test set-up

matic system for the vibration isolation table. A manual loading machine was mounted on the table on its side. The loading frame was rigidly connected to the table by two mechanical fixtures. A 3000 lb. (13.3 KN) load cell was used, along with tensile grips designed for the compact tension specimens. The first few holograms recorded showed fringe patterns corresponding to rigid body motions in the out-of-plane direction. To decrease that effect, two vertical steel fixtures were made. These fixtures with screws were used to restrict the right side loading arm from moving in the out-of-plane direction. Figure 5 a and b show the details of the mechanical set-up.

4.2 Test Specimen

Compact tension specimens were used. According to LEFM hypothesis, this type of specimen demonstrates unstable crack propagation, since the stress intensity factor (SIF) per unit load increases with an increase in crack length. Specimens were cut out of a large block of Indiana limestone. The blocks were cut into the specimen dimensions (6″ × 6″ × 1″), (15.24 cm × 15.24 cm × 2.54 cm) by a rotary diamond blade. A 2″ (5.1 cm) notch was cut into the specimens by the same saw. 1/2″ (1.27 cm) holes were then cored into the specimens by a diamond tipped core drill, with the hole center 1″ (2.54 cm) above the notch tip. A linear variable differential transducer (LVDT) was used to measure the crack mouth opening displacement during loading as per suggestions by Schmidt (1976). The LVDT was a highly sensitive miniature model with a linear range of 0.1″ (2.54 mm). It was mounted on the specimen with superglue adhesive (Fig. 5). The LVDT core was fixed to a rod which was screwed into a 1 cm × 1 cm aluminium block shown on the left side of the notch in Fig. 5. The screw-in arrangement made it easy to zero the LVDT after the adhesive hardened. Signal conditioners from "Kiethley Instruments" were used with the LVDTs. The local cell and LVDT outputs were monitored by "Fluke" multimeters.

5. Experimental Observations

Pre-peak or "slow" crack propagation from the original notch tip, could be detected both from the HI and ESPI observations. Figure 6 is a typical holographic fringe pattern which shows that the crack has propagated from the original notch tip prior to peak load. This crack propagation is visible as discontinuities in the fringe pattern in front of the notch tip. These crack growths start close to the load at which the Load-CMOD plot deviates from linear behavior (Fig. 7). Kinks in the displacement fringes signify strain concentrations. While the fringe patterns elsewhere in the specimen are continuous, they are distorted close to the crack tip, signifying higher strains in these regions. Strain or displacement readings cannot be directly obtained from this experiment.

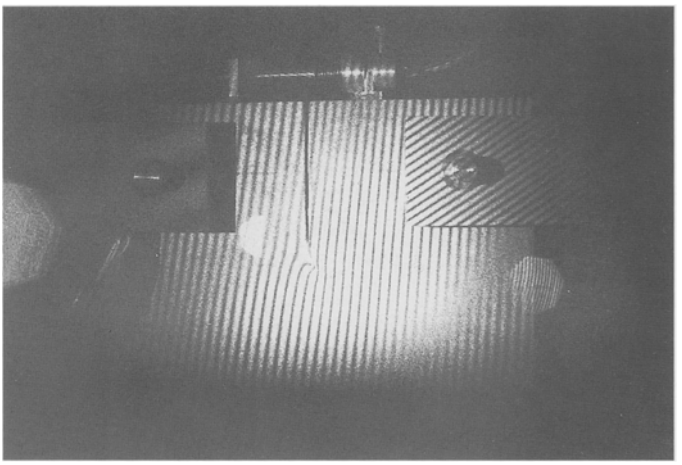

Fig. 6. Holographic interferometry fringe patterns

Figure 7 shows the load vs. CMOD of a typical specimen. All specimens tested failed with the crack propagating through the middle of the specimen as expected in a pure mode I type of fracture. Typical ESPI fringe patterns are shown in Fig. 8 a and 8 b. The quantitative measurement technique is shown in Fig. 8 a. If the fringes are counted from point C (light fringe) to a point A on the left side of the notch (dark fringe) the fringe count is 5.5 (count is 1 from a light fringe to the next light fringe). If the fringes are counted from the same initial point C to the point B (light fringe) (point corresponding to A across the notch), the count is 4.0. The fringe count on the left is greater by 1.5 fringes. Displacements are then measured using the equation:

$$d = n\lambda/(2 \sin \Omega), \tag{3}$$

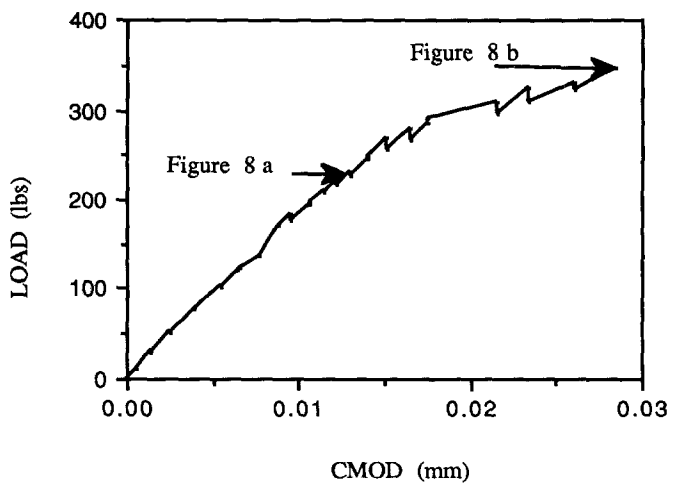

Fig. 7. Load vs CMOD measured by ESPI technique

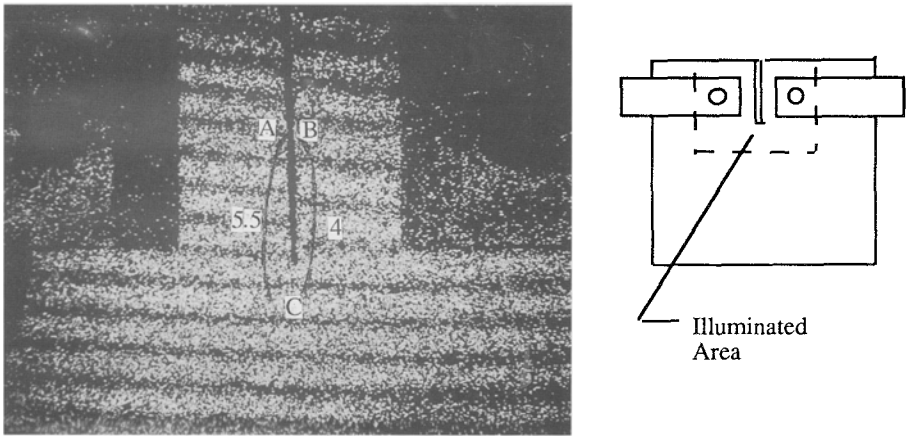

Fig. 8a. Speckle patterns observed by ESPI

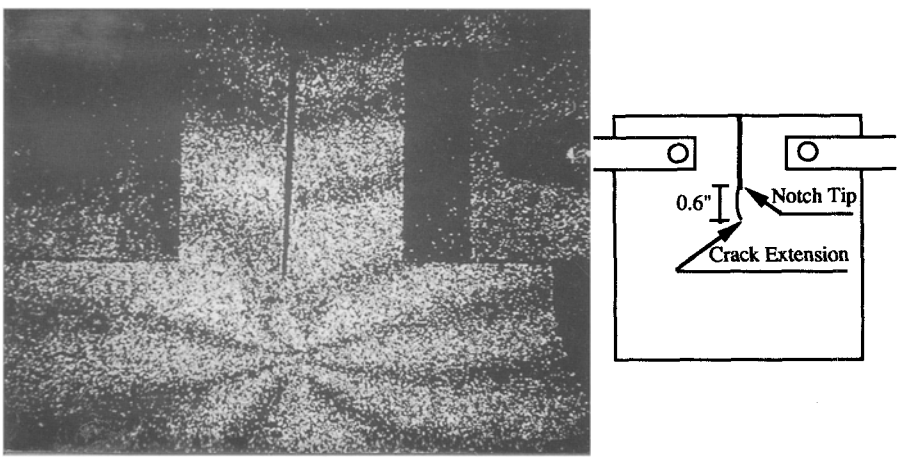

Fig. 8b. Prepeak crack propagation observed by ESPI

where d is the measured displacement, n is the difference in fringe counts ($= 1.5$) and Ω is the angle as shown in Fig. 4. This corresponds to an opening displacement of 0.67 micrometers between points A and B.

Figure 8b shows a stable crack propagation or "slow crack growth" of about 0.6″ (1.5 cm) (note the concentration of fringes ahead of the original notch tip) immediately prior to catastrophic failure observed by ESPI. This observation was similar to the earlier observation by HI. In Fig. 8a the fringes were straight and continuous because the displacement field was continuous. In Fig. 8b, the specimen is close to cracking and the displacement field is no longer continuous as seen from the curves and breaks in the fringe pattern at the crack tip. Since this technique offers real-time observation, it was possible to observe the propagation right up to unstable failure. All the three specimens tested with this technique

behaved similarly. The concentration of fringes in Fig. 8b shows the strain concentration at the propagated crack tip. The fringe discontinuities are primarily along the propagating crack, and very little distortion is observed in the surrounding region. This would indicate that the fracture process is localized along the crack. Figure 9 shows the crack opening profiles at different stages of loading as measured by ESPI.

In order to make more accurate observations in the region surrounding the crack, SEM studies were used. SEM micrographs are shown in Fig. 10a and 10b with magnifications of 81 and 380 respectively. Figure 10b is a magnification of the rectangular area marked in Fig. 10a. The crack is not continuously open. Tortuosity and ligament connections across the crack are evident in these pictures. Scanning the specimen at different regions in the vicinity of the crack, at magnifications of up to 1900 showed no presence of microcracking, and demonstrated no difference in microstructure between the regions near the crack or away from it.

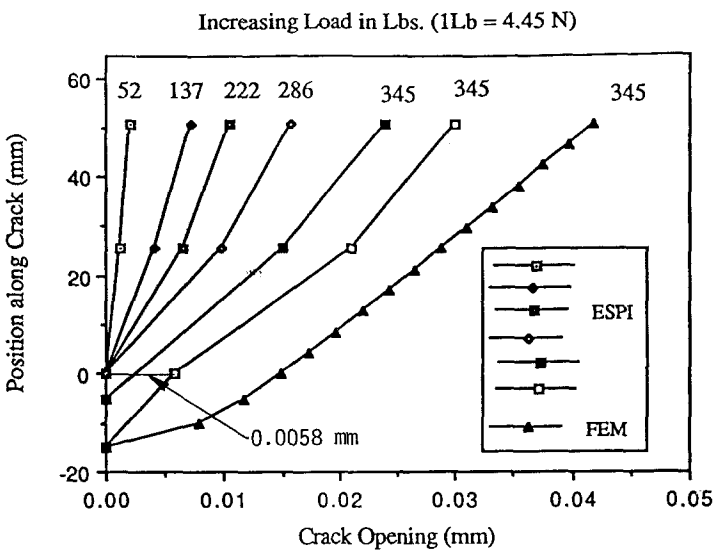

Fig. 9. Crack opening profile from ESPI and FEM

6. Finite Element Analysis

The experimental observations confirmed the existence of crack growth prior to peak load and the presence of crack bridging. Progressive crack growth was also accompanied by nonlinear response of the specimen. It is possible to explain the nonlinearity (increasing compliance of the specimen) as a result of crack growth.

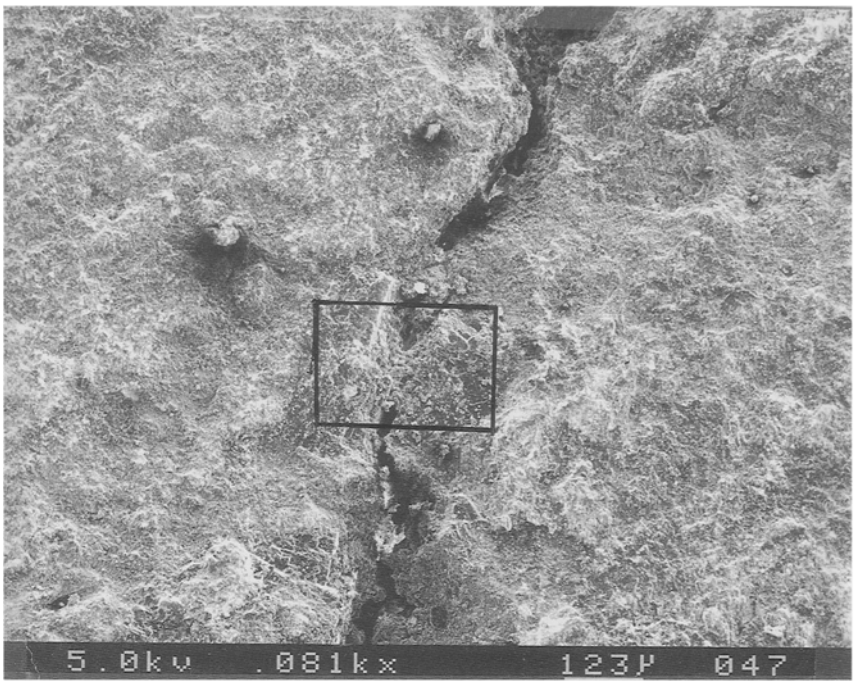

a

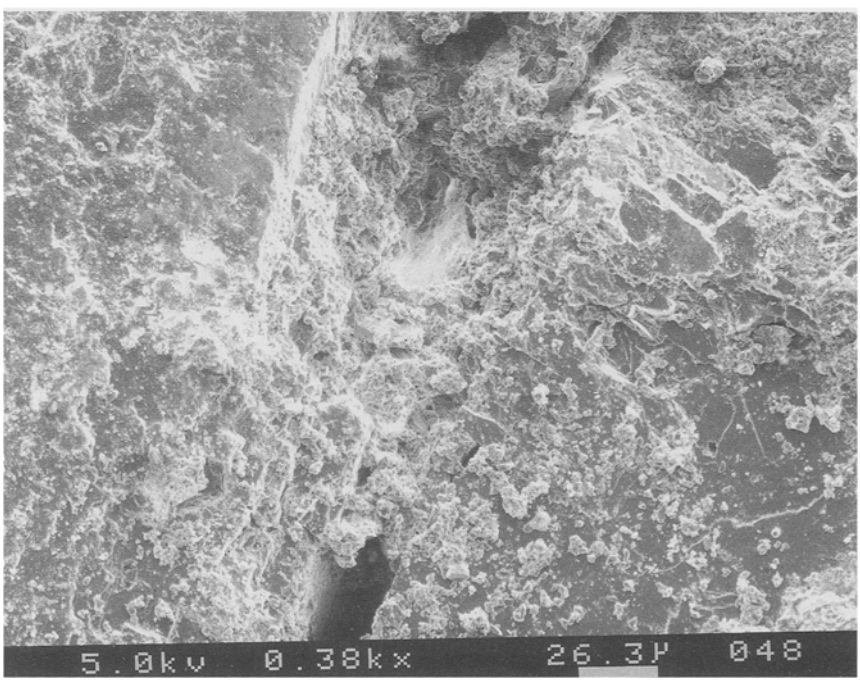

b

Fig. 10. Scanning electron microscopy (SEM) observations of the crack

Crack bridging can be modeled as shown in Fig. 11. A crack with ligament connections can be modeled as a crack without ligament connection, plus a crack with a closing pressure applied across the crack (Dugdale, 1960; Barenblatt, 1962; Labuz, 1985). This model is called the "closing pressure model". Both the application of this model and the measurement of compliance mentioned in the preceding paragraph, require using a finite element code, because no closed form solutions are available.

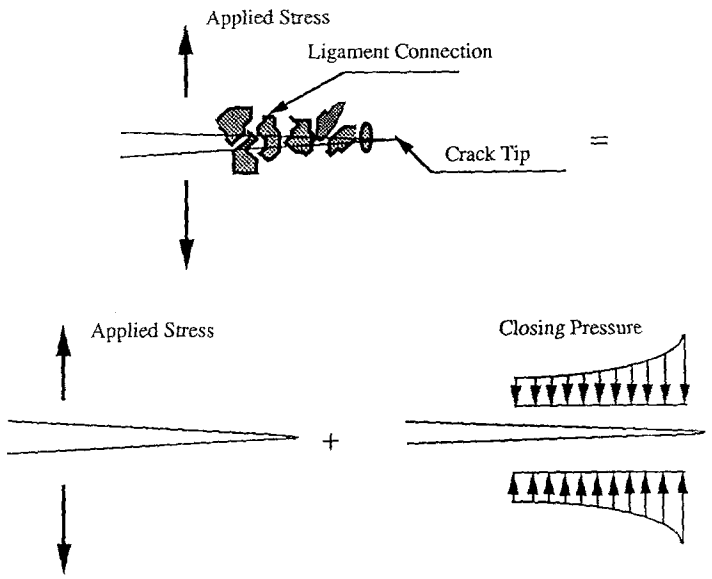

Fig. 11. Closing pressure model for ligament connection

6.1 Checking Accuracy of the Finite Element Program

An Interactive Finite Element (FEM) program developed at the University of New Mexico (Pantaki and Gerstle, 1988) was used to analyze the experimental results. Figure 12 shows a typical finite element mesh with quarter point singular elements used to analyze the specimen. As a first step in the analysis, the accuracy of the program with the described mesh was checked. To do this, the crack was progressively extended 0.2″ (0.51 cm) at a time. The stress intensity factor (SIF) and CMOD were calculated at each step for unit load. SIFs for unit load (for a traction free crack, i. e. no closing pressure involved) calculated using finite element analysis and closed form solutions by Tada (1973) and Hertzberg (1989) are plotted in Fig. 13. The FEM calculations were found to be in close agreement with the other results. In this figure, "a" is the vertical distance of the crack tip from the point of application of the load, and "w" is the vertical distance from the loading point to the bottom of the specimen (see inset in Fig. 13). K_I is the stress intensity factor caused by an applied load P.

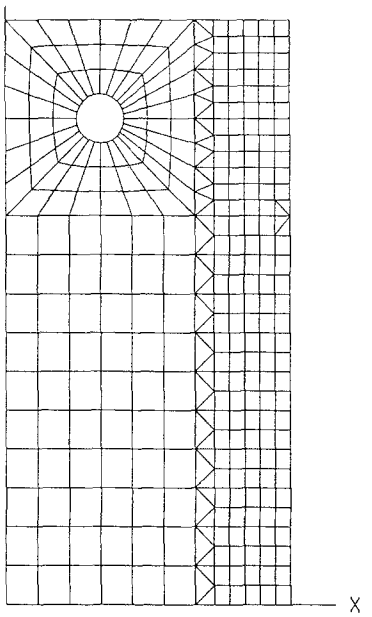

Fig. 12. Finite element mesh (FEM) used to analyze specimen

6.2 SIF and Compliance Calculations

The critical value of the SIF, K_{Ic}, was calculated to be 695 psi$\sqrt{\text{in}}$ (0.76 MPa$\sqrt{\text{m}}$) using the peak load in Fig. 7 and the FEM calculated value of the SIF for zero crack extension from Fig. 13. A value of 915 psi$\sqrt{\text{in}}$ (1.01 MPa$\sqrt{\text{m}}$) was obtained using the peak load and the extended crack length (0.6″, 1.52 cm), as was observed both from HI and ESPI.

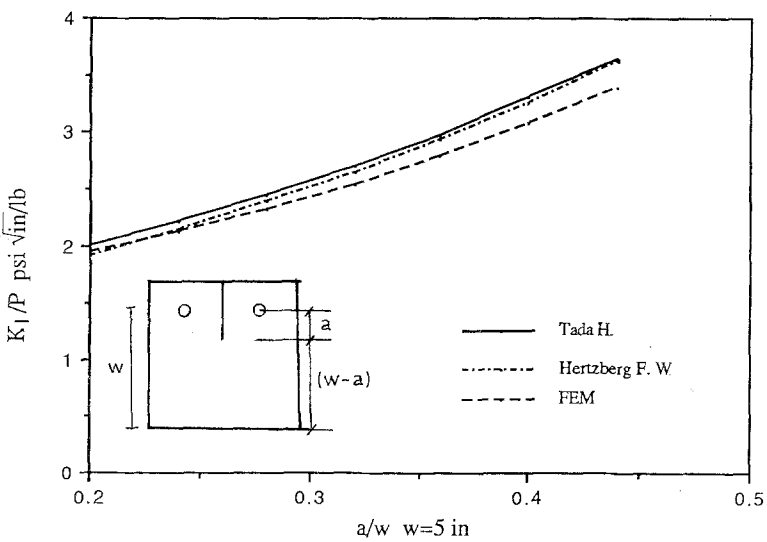

Fig. 13. Comparison of FEM results with theoretical formulae

From the initial linear portion of the load vs. CMOD behavior observed experimentally (Fig. 7), the value of the Young's Modulus of the limestone was calculated to be 4.5×10^6 psi., (31.0 GPa). If the material behaves elastically, then the change in compliance of the specimen (nonlinear behavior in Fig. 7) can be assumed to be due to the gradual propagation of the crack prior to peak load. Since E is known, the gradual increase in compliance was calculated by FEM, as the crack was progressively extended in the FEM mesh. The experimental peak load and corresponding CMOD were 350 lbs (1.56 KN) and 0.028 mm (Fig. 7). The FEM analysis showed that the crack had to extend by about 0.25″ (0.64 cm) to get a CMOD of 0.028 mm under the applied load of 350 lbs. (1.56 KN), as was observed experimentally. This meant that according to FEM, the crack had extended only 0.25″. This calculation assumed that the material was elastic, had the same value of E (31.0 GPa) as in the early stages of loading, and that there was no closing pressure on the crack face. This effective crack extension calculated by FEM analysis (0,25″, 0.64 cm) was smaller than the crack propagation observed on the surface by HI or by ESPI, which were about 0.6″ (1.52 cm). Maji and Shah (1988) have also reported that in concrete, the effective crack lengths obtained from compliance measurements are smaller than the crack extension observed experimentally. This discrepancy between FEM predictions and the experimental observations can be explained by the fact that no closing pressures were assumed in this analysis.

The crack openings displacements at the peak load (345 lbs., 1.53 KN) show that the experimental measurements with ESPI are different from the FEM predictions for crack opening displacements (Fig. 9). The FEM crack opening displacements were obtained using a 2.6″ (6.6 cm) crack length without any closing pressure and with $E = 4.5 \times 10^6$ psi (31.03 GPa). Hence, the experimentally observed openings are smaller than that predicted using a traction-free crack length. This also indicates that traction forces should be incorporated in the FEM analysis to better predict experimental observations.

6.3 Implementing the Closing Pressure Model in FEM

Next, the effect of traction forces on the stress intensity factor was investigated using the closing pressure model. These traction forces existed only on the extended portion of the crack, since the initial notch was sawed, and did not have any grain bridging. Since the magnitude of the closing pressure was not known, the following analysis was performed:

It is expected that the closing pressure or stress transferred due to crack bridging would depend on the opening of the crack. In the absence of any other data, we attempted to estimate the magnitude of this closing pressure from the stress vs. crack opening relation of specimens tested in uniaxial tension. Figure 14a shows a typical stress vs. displacement data of a Charcoal Granite specimen (Labuz et al., 1985). These data were used

since no data were available on the strain softening behavior of limestone or of rocks of similar grain size.

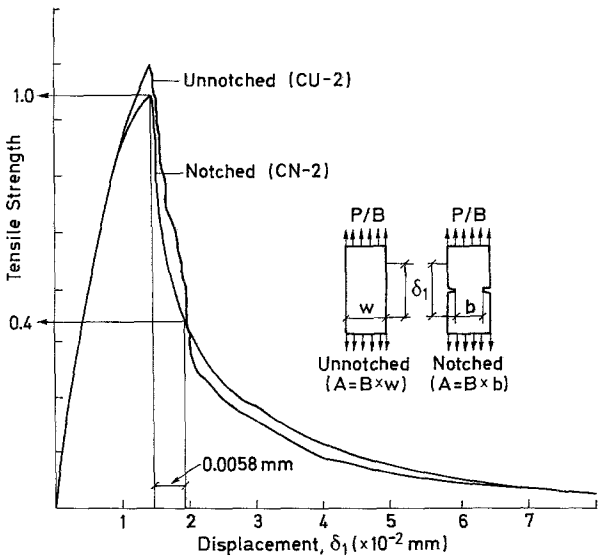

Fig. 14a. Load-displacement behavior of charcoal granite (Labuz; 1985)

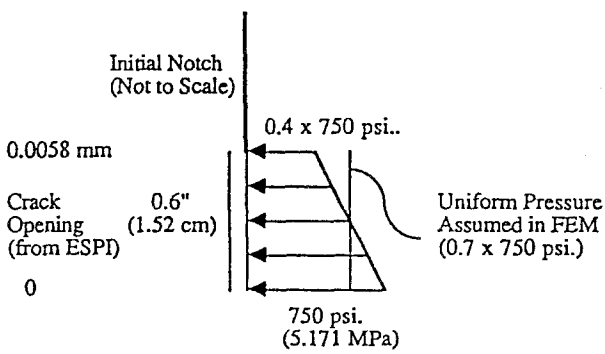

Fig. 14b. Traction forces based on measured displacements

In our experiment, the original notch tip opened by 0.0058 mm at peak load (Fig. 9). From Fig. 14a, when the crack opens by 0.0058 mm, the stress transferred drops to about 0.4 of the tensile strength. Hence, the traction on the propagated portion of our crack could be approximated as shown in Fig. 14b. It is equal to the tensile strength at the crack tip, where the crack opening is zero, and is 0.4 times the tensile strength at the original notch tip where the crack opening is 0.0058 mm (see Fig. 14a). To simplify the computations, a uniform closing pressure was assumed. The tensile

strength was assumed to be 750 psi ($\sigma = 750$ psi., 5.17 MPa) (Schmidt, 1976). The uniform cohesive crack closure stress was calculated by distributing the varying pressure uniformly along the extended crack (see Fig. 14a) as:

$$(1.0\,\sigma + 0.4\,\sigma)/2 = 0.7\,\sigma = 0.7 \times 750 \text{ psi.} = 525 \text{ psi } (3.62 \text{ MPa}).$$

The effect of the traction forces on the extended portion of the crack was calculated using FEM. To do that, the nodes from the crack tip to the original notch tip (length of 0.6″) were loaded with the uniform closing pressure of 3.62 MPa calculated above. The SIF due to this closing pressure was 781.2 psi$\sqrt{\text{in}}$ (or 0.858 MPa/m).

The resulting SIF due to the external load (0.76 MPa$\sqrt{\text{m}}$ and 1.01 MPa$\sqrt{\text{m}}$) and that due to the closing pressure model (or 0.858 MPa/m) would therefore seem to produce a net SIF of almost zero or negative. This is not consistent with available experimental data reported by others. A longer crack length is likely to produce a negative SIF, or a stable crack growth all through the specimen. This was not experimentally observed for this specimen, which reached peak load with a crack extension of only 0.6″ (1.52 cm) and then failed in an unstable manner. Attempts have been made to evaluate the stress transferred across a crack by measuring the decrease in the strength of rocks after the peak load (Fig. 14a), called "strain softening" (Labuz et al., 1985). The calculations reported here seem to suggest that one needs to obtain more realistic data on the stress transferred in the cohesive zone. Such stresses are likely to be significantly smaller than the tensile strength of the rock, or the stress vs. crack opening data obtained from the strain softening behavior. More accurate FEM calculation and modeling of nodal forces would have made the numbers obtained above more accurate, but would not change the nature of the results.

7. Conclusions

1. Holographic Interferometry was used to study pre-peak crack growth in Limestone using an unstable crack propagation geometry. Stable crack propagation and growth of the fracture process zone could be observed from distortions in the holographic fringe patterns.

2. Electronic Speckle Pattern Interferometry was used for quantitative measurement of displacement profiles along the crack, and for real-time monitoring of the fracture process. The crack profiles were useful in determining the effect of traction forces on the process zone.

3. Experimental observations suggested that ligament connection or stress transfer along the propagating crack is the dominant feature of the process zone.

4. Studies using a scanning electron microscope demonstrated crack bridging, but did not show any presence of microcracking in the process zone.

5. Stress intensity factors for Indiana limestone were calculated. Experimental measurements of load vs. crack opening displacements were compared with those from FEM analyses assuming no closing pressure on the crack. The resulting "effective crack length" in the FEM analysis was much smaller than the crack extension length observed by interferometry. This suggests the presence of ligament connection and the necessity of using a closing pressure model.

6. FEM calculations including crack-face tractions to model closing pressure indicated that the traction forces had to be significantly smaller than the tensile strength of the material, for even small crack openings. Very limited experimental information is available on cohesive zone models for rocks and additional research is required in this area. Critically considering the crack opening displacements, the interferometry techniques described here may be extremely useful for obtaining some of the necessary data.

Acknowledgement

This research was funded by the Sandia University Research Program (SURP), to the University of New Mexico, supported by the Sandia National Laboratory, under contract no. 3-13496. The support and suggestions of Dr. Wolfgang Wawersik are gratefully acknowledged. The authors also acknowledge Professor M. L. Wang, W. Gerstle and T. Ross for assistance on different aspects of the project.

References

Ballarini, R., Shah, S. P., Keer, L. M. (1984): Crack growth in cement based composites. Engng. Fract. Mech. 20 (3), 433—446.

Barenblatt, G. I. (1962): Mathematical theory of equilibrium cracks in brittle fracture. Adv. Appl. Mech. 7, 55—129.

Bazant, Z. P. (1985): Mechanics of fracture and progressive cracking in concrete structures. In: Shi, DiTommaso (eds.), Fracture mechanics of concrete, Martinus Nijhoff, Dordrecht, 1—94.

Boone, N., Wawrzynek, P. A., Ingraffea, A. (1986): Simulation of the fracture process in rock with application to hydrofracturing. Int. J. Rock Mech. Min Sci. 23 (3), 255—265.

Butters, J. N., Leendertz, J. A. (1971): Speckle pattern and holographic techniques in engineering metrology. Opt. Laser Technol. 3 (1), 26—30.

Chhuy, S., Cannard, G., Robert, J. L., Acker P. (1986): Experimental investigation into the damage of cement concrete with natural aggregates. In: Brandt, A. M., Marshall, I. H. (eds.), Brittle matrix composites 1, Elsevier, Amsterdam, 341—353.

Diamond, S., Bentur, A. (1985): On the cracking of concrete and fibre reinforced cements. In: Shah, S. P. (ed.), Application of fracture mechanics to cementitious composites, Martinus Nijhoff, Dordrecht, 87—141.

Du, J., Hawkins, N. M., Kobayashi, A. S. (1989): A hybrid analysis of fracture process zone in concrete. In: Shah, S. P., Swartz, S. E. (eds.), Fracture of concrete and rock: Recent developments, Elsevier, Amsterdam, 297—306.

Dugdale, D. C. (1960): Yielding of steel sheetings containing slits. J. Mech. Phys. Solids 8, 100—104.

Getting, I. C., Roecken, C., Spetzler, H. (1986): Improved acoustic emission locations. J. Nondestructive Evaluation 5 (3/4), 133—143.

Griffith, A. A. (1921): The phenomena of rupture and flow in solids. Philosophical Transactions, Series A, vol. 221, Royal Soc. London, 163—198.

Hertzberg, F. W. (1989): Deformation and fracture mechanics of engineering materials. 3rd ed., Wiley, New York, 655.

Hoagland, R. G., Hahn, G. T., Rosenfield, A. R. (1973): Influence of microstructure on fracture propagation in rock. Rock Mechanics 5 (2), 77—106.

Jacquot, P., Rastogi, P. K. (1983): Speckle metrology and holographic interferometry applied to the study of cracks in concrete. In: Wittmann, F. H. (ed.), Fracture mechanics of concrete, Elsevier, Amsterdam, 113—156.

Jenq, Y. S., Shah, S. P. (1985): A fracture toughness criterion for concrete. Engng. Fract. Mech. 21 (5), 1055—1069.

Jones, R., Wykes, C. (1983): Holographic and speckle interferometry. Cambridge University Press. 165—197.

Kobayashi, T., Fourney, W. I. (1978): Experimental characterization of the development of the microcrack process zone at a crack tip in rock under load. In: Proc., 19th U. S. Symp. on Rock Mech., Nevada, Reno, 243—246.

Labuz, J. F., Shah, S. P., Dowding, C. H. (1985): Experimental analysis of crack propagation in granite. Int. J. Rock Mech. Min. Sci. 22 (2), 85—98.

Maji, A. K., Shah, S. P. (1988): Process zone and acoustic emission measurements in concrete. Experimental Mechanics, March, 27—33.

Maji, A. K., Shah, S. P. (1989): Application of acoustic emission and laser holography to study microfracture in concrete. ACI-SP 112, Nondestructive Testing, American Concrete Institute, 83—107.

Maji, A. K., Shah, S. P. (1990): Measurement of mixed-mode crack profiles by holographic interferometry. Experimental Mechanics, June, 201—207.

Maji, A. K., Shah, S. P. (1991): Laser interferometry methods. RILEM Committee 89-FMT Report, Fracture mechanics of concrete: Test methods, RILEM, France, 263—279.

Miller, R. A., Shah, S. P., Bjelkhagen, H. I. (1988): Crack profiles in mortar measured by holographic interferometry. Experimental Mechanics, December. 388—394.

Mindess, S. (1983): The application of fracture mechanics to cement and concrete: a historical review. In: Wittmann, F. H. (ed.), Fracture mechanics of concrete. Elsevier, Amsterdam, 1—41.

Mindess, S. (1991): Fracture process zone detection. RILEM Committee 89-FMT Report, Fracture mechanics of concrete: Test methods, RILEM, France, 231—262.

McClintock, F. A., Irwin, G. R. (1965): Plasticity aspects of fracture mechanics, fracture toughness testing and its applications. ASTM STP 381, p. 84.

Najjar, W. D., Hover, K. C. (1988): Modifications of the X-radiography technique to include a contrast agent for identifying and studying microcracking in concrete. Cement, Concrete and Aggregate 10 (1), 15—19.

Nolen-Hoeksema, R. C., Gordon, R. B. (1987): Optical detection of crack patterns in the opening-mode fracture or marble. Int. J. Rock Mech. Min. Sci. and Geomech. Abstr. 24 (2), 135—144.

Ouchterlony, F. (1982): Review of fracture toughness testing of rock. SM Archives 7, Martinus Nijhoff Publishers, Dordrecht, 131—211.

Pantaki, M. J., Gerstle, W. (1988): A new integrated, computer graphics design tool. Technical Report RSI-039, NSF-SBIR phase I Report, Washington.

Park, D., Jung, J. (1988): Application of holographic interferometry to the study of time-dependent behavior of rock and coal. Rock Mech. Rock Engng. 21 (4), 259—270.

Regnault, P., Bruhwiler, E. (1988): Holographic interferometry for the determination of fracture process zone in concrete. In: Proc., Int. Conf. Fracture of Concrete and Rock, Vienna.

Rossmanith, H. P. (ed.) (1983): Rock fracture mechanics. Springer, Wien New York, 69—150.

Schmidt, R. A. (1976): Fracture toughness testing of limestone. Experimental Mechanics 16, 161—167.

Schmidt, R. A., Lutz, T. J. (1979): K_{Ic} and J_{Ic} of westerly granite — effects of thickness and In-plane dimensions. In: Freiman, S. W. (ed.), Fracture mechanics applied to brittle materials, ASTM, STP 678, Philadelphia, 166—182.

Swanson, P. L. (1984): Subcritical fracture propagation in rocks: An examination using methods of fracture mechanics and nondestructive testing. PhD Dissertation, University of Colorado, Boulder.

Tada, H. (1973): The stress intensity factor handbook. Del Research Corporation, Hellertown, Pa.

Author's address: Dr. A. K. Maji, Department of Civil Engineering, University of New Mexico, Albuquerque, NM 87131, U. S. A.